3D CFD CONV CODE: VALIDATION AND VERIFICATION

V.V. Chudanov[1], A.E. Aksenova[1], V.A. Pervichko[1], A.A. Makarevich[1], N.A. Pribaturin[2], O.N. Kashinskii [2]

[1]Nuclear Safety Institute, RAS, Moscow 115191,52 B.Tulskaya, Russia
Institute of Thermophysics, Siberian Branch of RAS, Novosibirsk 630090, Russia

Abstract

During some years in IBRAE a set of 3D CFD modules (CONV code) for safety analysis of the operated Nuclear Power Plants (NPPs) is developing. These modules are based on the developed algorithms with small scheme diffusion, for which the discrete approximations are constructed with use of finite-volume methods and fully staggered grids. The CONV code is fully parallelized and highly effective on high performance computers. The developed modules were validated on a series of well known tests in a wide range of Rayleigh numbers (10^6-10^{16}) and Reynolds numbers (10^3-10^5). In this paper the examples of use of the developed software for modeling a fuel assembly, namely, for researching a hydraulic resistance factor of a spacer, are demonstrated. The calculations are carried out on a sequence of condensed grids with an amount of nodes from a range 10^7-10^8, for which the convergence was obtained. Moreover, the attention of this paper is focused on validation and verification of the software with usage of such tests as: 3D convection in a lid-driven cavity flow, turbulent flow of water in a round pipe, backward-facing step flow and T-junction thermal mixing test. In all cases a good agreement was obtained.

1. INTRODUCTION

At 21 century IAEA (Modro, 2006) is focused on two new directions, bound with an estimate of safety. These concern the issue of uncertainties in deterministic evaluation of safety, and the role of CFD methods in safety assessments. The current trend in accident analysis is to use best estimate computer codes. However, these codes are typically one dimensional approximation of phenomena and plant systems. These methods are not adequate for some applications, particularly where modeling local flow and heat transfer phenomena is important to safety. There is therefore increasing interest in the application of three dimensional computational fluid dynamics (CFD) codes for safety analysis as a supplement to or in combination with system codes. It is noted that CFD codes are capable of calculating local parameters. Due to this capability they provide insights into many problems, contribute to a deeper understanding of flow physics, and thus may lead to better designs at reduced cost and/or to more precisely quantified safety margins (Modro, 2006).

During some years in IBRAE, a 3D unified numerical thermalhydraulic technique for safety analysis of the operating NPPs is developing, which includes: 1) methods, algorithms and software for automatic generation of computing grids with local refinement near body borders, 2) methods and algorithms for solving the heat and mass transfer in compressible/incompressible problems for research of 3D thermalhydraulic phenomena, 3) approaches for modeling of turbulence. Briefly we shall stop on details of the developed approach.

For the grid construction in IBRAE, an automatic technology using CAD systems for designing of calculated domain is developed. A generation of structured orthogonal/Cartesian grids with a local refinement near boundaries is incorporated into a specially developed program, which is supplied by a friendly interface and can be utilized on parallel computers (Chudanov, 1999).

A computing technique is based on developed algorithms with small scheme diffusion, for which the discrete approximations are constructed with the use of finite-volume methods and fully staggered grids.

For the modeling of 3D turbulent single-phase flows, an LES approach (commutative filters) and also a quasi direct numerical simulation (QDNS) approach are used. For the simulation of 3D turbulent two-phase flows by means of DNS, detailed enough grids and effective numerical methods developed in IBRAE for solving CFD problems are applied. For observation of an interface of two-

phase flow, the modified level set (LS) methods and multidimensional advection/convection schemas of total variation diminishing (TVD) type with small scheme diffusion with use of sub-grid simulation (with local resolution) are used.

A developed numerical technique was used for the construction of the 3D CFD CONV code (set of numerical modules) for safety analysis of the operated Nuclear Power Plants (NPPs). Therefore further, without loss of generality, we shall speak about singularities validation and verification of a numerical technique, i.e. developed modules. The developed modules were validated on a series of well known tests in a wide range of Rayleigh numbers (10^6-10^{16}) and Reynolds numbers (10^3-10^5). In this paper the examples of use of the developed software for modeling of a fuel assembly, namely, for researching a hydraulic resistance factor of a spacer, are demonstrated. The calculations are carried out on a sequence of condensed grids with an amount of nodes from a range 10^7-10^8, for which the convergence was obtained. Moreover, the attention of this paper is focused on validation and verification of the software with usage of such tests as: 3D convection in a lid-driven cavity flow, turbulent flow of water in a round pipe, backward-facing step flow and T-junction thermal mixing test.

2. CFD NUMERICAL TECHNIQUES

This section deals with the new methods and algorithms for describing of 3D thermalhydraulic processes at NPPs. Among them we consider numerical algorithms for solving of incompressible fluid dynamics, the monotone multi-dimensional schemes of TVD-type for solving of advection equation and the effective algorithm for solving of the elliptical equation for pressure correction.

To simulate thermalhydraulic in incompressible media, the time-dependent incompressible Navier-Stokes equations in the primitive variables [3] coupled with the energy equation are used:

$$\begin{cases} \dfrac{d\rho\bar{v}}{dt} = -\operatorname{grad} P + \operatorname{div}\nu \operatorname{grad}\bar{v} + \rho g + \mathrm{CSF}, \\ \operatorname{div}\bar{v} = 0 \end{cases} \tag{1}$$

$$\frac{\partial(\rho h)}{\partial t} + \operatorname{div}(\rho v h) = \operatorname{div}(k \operatorname{grad} T); \quad h = \int_0^T c(\xi)\, d\xi\,. \tag{2}$$

Basic features of developed numerical algorithm (Chudanov, 2003, 2005) incorporated in the present approach are the following:

Numerical implementation of operator-splitting scheme for the Navier-Stokes equations is performed as the predictor-corrector procedure with correction for the pressure:

$$\rho\frac{\mathrm{v}^{n+1.2} - \mathrm{v}^n}{\tau} + (C(v) - \operatorname{div}\nu \operatorname{grad})\mathrm{v}^{n+1/2} + \operatorname{grad} p^n - \mathrm{CSF}^n = 0,$$

$$\operatorname{div}_h\left(\frac{1}{\rho}\operatorname{grad}_h \delta p\right) = \frac{1}{\tau}\operatorname{div}_h \mathrm{v}^{n+1/2}, \qquad \mathrm{v}^{n+1} = \mathrm{v}^{n+1/2} - \frac{\tau}{\rho}\operatorname{grad}_h \delta p\,. \tag{3}$$

To construct time-integration scheme for the energy equation, its operators are decomposed into two parts associated with the enthalpy and temperature respectively, that results in the following two-step procedure:

$$\frac{h^{n+1/2} - h^n}{\tau} + \tilde{C}\left(\mathrm{u}^n\right)h^{n+1/2} = 0, \quad \frac{h^{n+1} - h^{n+1/2}}{\tau} - \tilde{N}\,T^{n+1} = 0. \tag{4}$$

In the momentum equation, operators are also splitted into two parts. The first part is associated with the velocity transport by convection/diffusion written in the linearized form as $A_1 = C\left(\mathrm{u}^n\right) + N$, where $N = \operatorname{div}\left(\frac{\mu}{\rho}\operatorname{grad}\mathrm{v}\right)$. The second part deals with pressure gradient $A_2 = \operatorname{grad}$. It should be noted that the gradient and divergence operators are adjoint of each other, i.e. $A_2^* = -\operatorname{div}$.

The analyzed additive scheme of splitting looks like:

$$\frac{\mathrm{v}^{n+1/2} - \mathrm{v}^n}{\tau} + A_1\mathrm{v}^{n+1/2} + A_2 p^n = f^n, \frac{\mathrm{v}^{n+1} - \mathrm{v}^n}{\tau} + A_1\mathrm{v}^{n+1/2} + A_2 p^{n+1} = f^n, A_2^*\mathrm{v}^{n+1} = 0. \tag{5}$$

Numerical implementation of this scheme is performed as the predictor-corrector procedure, i.e. introducing the pressure correction $\delta p = p^{n+1} - p^n$ in two last equations (5) allows to receive the well-known Poisson equation and equation for velocity correction in form:

$$\mathrm{div}_h \mathrm{grad}_h \delta p = \frac{1}{\tau}\mathrm{div}_h \mathrm{v}^{n+1/2}, \quad \mathrm{v}^{n+1} = \mathrm{v}^{n+1/2} - \tau \mathrm{grad}_h \delta p \ .$$

The Fast Fourier Transformation is applied for solving of the selfadjoint and self-consistent grid elliptic problem for pressure that allows achieving high speed of computing algorithm in comparison with the standard approaches.

In computational mathematics there are recognized two variants of fictitious domain methods with continuation of coefficients at lower-order derivatives and with continuation of coefficients at the highest-order derivatives. Both approaches are in common use for prediction of fluid dynamics with phase change processes.

Here the first variant is employed which in physical sense can be considered as inclusion into the momentum equations of model of a porous medium:

$$\frac{\partial \mathrm{v}_\varepsilon}{\partial \tau} + C(\mathrm{v}_\varepsilon)\mathrm{v}_\varepsilon - \mathrm{div}\left(\frac{\mu}{\rho}\,\mathrm{grad}\,\mathrm{v}_\varepsilon\right) + \mathrm{grad}\ p + c_\varepsilon \mathrm{v}_\varepsilon = \mathrm{f}_\varepsilon,$$

$$\mathrm{div}\ \mathrm{v}_\varepsilon = 0 \qquad (6)$$

where p - pressure, normalized on the density. Various formulae of c_ε can be employed for the flow resistance term in the above equations. For equation (6) the modified predictor-corrector procedure with taking into account of fictitious domain method looks like this:

$$\frac{\mathrm{v}_\varepsilon^{n+1/2} - \mathrm{v}_\varepsilon^{n}}{\tau} + A_1 \mathrm{v}_\varepsilon^{n+1/2} + A_2 p_\varepsilon^n + c_\varepsilon \mathrm{v}_\varepsilon^{n+1/2} = \mathrm{f}^n,$$

$$\mathrm{divgrad}\ \delta \mathrm{p}^{s+1} = \mathrm{div}_h \left(\frac{\tau c_\varepsilon}{1+\tau c_\varepsilon}\mathrm{grad}_h\ \delta p^s\right) + \frac{1}{\tau}\mathrm{div}_h\ \mathrm{v}_\varepsilon^{n+1/2},$$

$$\mathrm{v}_\varepsilon^{\mathrm{n+1}} = \mathrm{v}_\varepsilon^{\mathrm{n+1/2}} - \frac{1}{1+\tau c_\varepsilon}\mathrm{grad}_h\ \delta p_\varepsilon.$$

For solving of convection problem the regularized nonlinear monotonic operator-splitting scheme was developed (Chudanov, 2001). The special approximation of convection terms $C(\mathrm{v})$ are employed in order to derive the discrete convective operator, which is skew-symmetrical and does not give any contribution to the kinetic energy (i.e. energetically neutral (Chudanov, 2001)).

So, this scheme provides the second order in space and the first one in time. The algorithm is stable at a large enough integration step by time. Details of the validation of the presented approach on a wide set of both 2D and 3D tests are reported in (Chudanov, 1998). New verification and validation results are presented in the next sections.

3. VERIFICATION ASPECT

The developed technique was verificated by means of the theoretical analysis of major phenomena such as boundary layers formation together with the analysis of energy balance in heat generating fluids. Theoretical dependences were compared with numerical results of such processes as: free convection in a heat–generating fluid for cylindrical geometry; convective heat exchange for a heat-generating fluid in an upper of enclosure.

3.1 Analysis of a free convection in a heat–generating fluid for cylindrical geometry

The characteristics of a stationary free convective heat exchange in a heat-generating fluid placed in a cylindrical volume are investigated by the method of analytical estimations (Bolshov, 1998) at Prandtl number ~1. It is shown that in the lower part of a basic volume (outside of a vertical boundary layer=BL) a steady-state temperature stratification exists down to the bottom of the cylinder. In this field the dependence of temperature versus H is an exponential function. Densities of heat flux to lateral boundary q_{sd} (in a place higher than a level of the horizontal BL) and one to the lower

horizontal boundary of volume q_{dn} practically are constant. At large values of modified Rayleigh number Ra_l there are strongly difference in densities from each other:

$q_{sd}/q_{dn} \sim Ra_l^{1/9} >> 1$.

At intersections of vertical BL with lower horizontal BL, the heat flux increases sharply with height by the linear law from q_{dn} up to q_{sd}.

3.2 Boundary layer to the lateral wall

For this problem analytical estimations for distribution of temperature in interior volume (Bolshov, 1998) were obtained in form

$$u \sim u_0\left(\frac{z}{H}\right)^{3/5}, \quad \delta_{sd} \sim \delta_0\left(\frac{z}{H}\right)^{1/5}, \quad T_b \sim T_0\left(\frac{z}{H}\right)^{1/5}, \quad V_z \sim V_{z_0}\left(\frac{z}{H}\right)^{4/5},$$

where $u_0, V_{z_0}, \delta_0, T_0$ - are the corresponding values of velocities, thickness of boundary layer and temperature at a level z~H.

The temperature in the basic volume and the BL thickness have identical dependence on longitudinal coordinate. Therefore the density of heat flux to a lateral wall is defined as:

$$q_{sd} \sim \frac{\lambda T_b}{\delta_{sd}} \sim \frac{\lambda T_0}{\delta_0} \sim q_{sd_0} = const\,.$$

Here λ - heat conductivity, q_{sd0} – density of heat flux to a lateral wall at level z~H. Thus, the heat flux to the lateral wall reaches stationary values in δ_{dn}<<z<<H, where δ_{dn} – thickness of lower horizontal BL.

Direct Numerical Simulation has been carried out in case of a cylindrical geometry with adiabatic upper and isothermal lateral boundaries for $Ra=10^8$-10^{12} (see fig.1a). By symmetry, the results are presented for a one-half of cylindrical geometry with adiabatic upper, isothermal right/lower boundaries. The left boundary is a symmetry axis. Mesh resolution corresponds to Kolmogorov's scale. The numerical estimate of heat fluxes in BL in δ_{dn}<<z<<H is close to a constant that coincides with theoretical analysis (Bolshov, 1998). The predicted heat flux in the boundary layer on the lateral boundary near of zero has the explicitly expressed linear dependence (fig.1c - red fragment), i.e. for $z \le \delta_{dn}$ we have:

$$\delta_{sd} \sim const, \quad q_{sd} \sim q_{sd_0}\left(\frac{z}{\delta_{dn}}\right).$$

Then the character of the predicted flux varies on almost horizontal in a range of heights from 0.2 up to 0.3 (fig.1c - blue fragment). That completely corresponds to the results of the theoretical analysis (Bolshov, 1998).

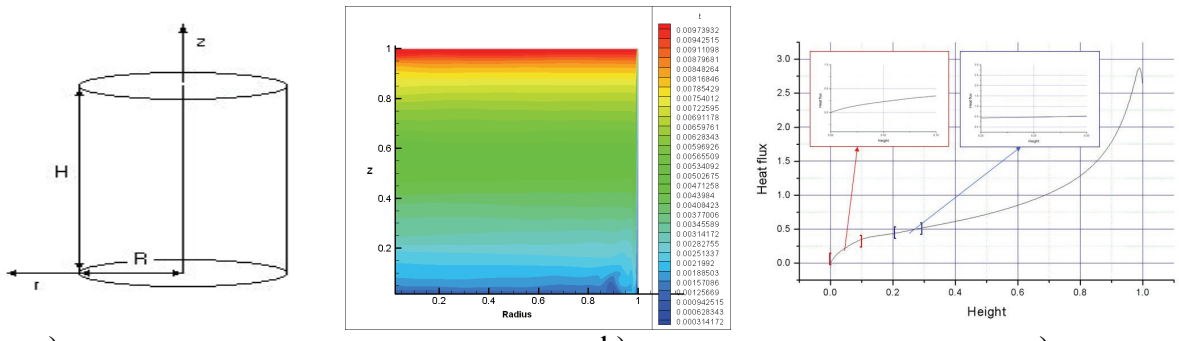

a) b) c)

Fig.1: a) Sketch; b) Isotherms at $Ra=10^{12}$. b) Heat flux versus height.

The vertical BL perceives the horizontal one as a motionless liquid. It is well visible from fig.2, where the lower fragment from fig.1b is shown. At the right boundary a downward flow towards bottom is observed. Along lower cold boundary the horizontal BL is observed. Where the BL interaction is take place, an eddy in a lower right angle occurs.

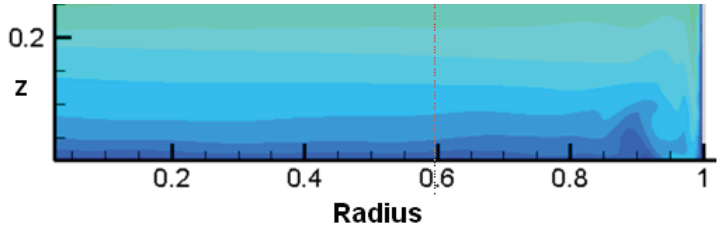

Fig.2: The eddy in a lower right angle of domain at Ra=10^{12} .

3.3 Boundary layer on the bottom

The theoretical analysis of boundary layer on the bottom (Bolshov, 1998) supposes that, the steady stratification is kept (to within $O\left(\frac{\delta_{dn}}{R}\right)^2$) down to the bottom of the cylinder. A ratio of densities of heat flux is inversely proportional to the ratio of the appropriate BL's thickness:

$$\frac{q_{dn}}{q_{sd}} \sim \frac{\delta_{sd}}{\delta_{dn}}.$$

Density of a heat flux to the lower horizontal boundary appears constant, it is a much smaller density of heat flux to a vertical wall at $z \geq \delta_{dn}$:

$$\frac{q_{dn}}{q_{sd}} \sim \left(\frac{\delta_0}{R}\right)^{5/9}\left(\frac{R}{H}\right)^{1/9} << 1$$

For thickness of the BL on the lateral wall at z~H we shall receive:

$$\delta_0 \sim HRa_I^{-1/5}$$

The density ratio of heat fluxes to the lower and lateral boundaries looks like:

$$r(Ra) = q_{dn} \Big/ q_{sd_0} \sim Ra_I^{-1/9}.$$

For different Ra numbers the characteristic values of r(Ra) are presented in table:

Table1: the characteristic values of r(Ra)

Ra	10^8	10^9	10^{10}	10^{11}	10^{12}
Theory, r(Ra)	0.129	0.100	0.071	0.057	0.044
Numerical Predictions	0.125	0.095	0.076	0.058	0.048

Thus, the ratio of r(Ra) equals:

$$\frac{r(10^8)}{r(10^9)} \approx \frac{r(10^9)}{r(10^{10})} \approx \frac{r(10^{10})}{r(10^{11})} \approx 10^{1/9}.$$

The numerical predictions of heat fluxes at the lateral and lower boundary in BL are in good correspondence with results of theoretical analysis (Bolshov, 1998).

3.4 Convective of a cooling down fluid without interior heat sources

For this problem analytical estimations for distribution of temperature in interior volume (see Bolshov, 2001) were obtained in form

$$T_b(z,t) = T_0(t)\exp\left(k\frac{z}{R}\right)$$

where T_0- temperature value, counted form the temperature on the boundary, z – coordinate, counted from a pole level ($\theta = 0$) on a vertical upwards, R – radius of a boundary curvature, t – time, k – dimensionless value.

At figure 3a the results of direct numerical simulation in comparison with analytical estimations (Bolshov, 2001) for distribution of temperature in interior volume are submitted. As it is possible to see from figure, the good enough coincidence of numerical predictions to analytical estimations is observed.

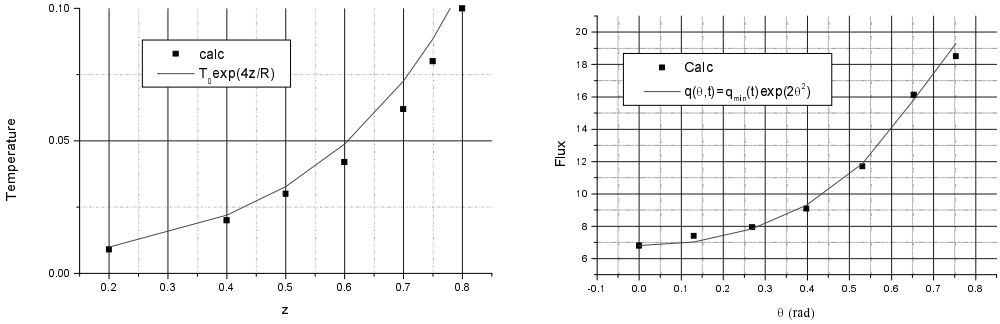

a) b)

Fig.3: a) Temperature distribution in internal volume, where k=4. b) Heat flux density distribution on a boundary, where p=2.

For this test analytical estimations of heat flux density distribution on a boundary (see Bolshov, 2001) were obtained also in form

$$q(\theta,t) = q_{\min}(t)\exp\left(p\theta^2\right),$$

where θ - angle, q_{min}- minimum value of heat flux density on boundary realized under θ=0, t - time, p – dimensionless parameter.

At figure 3b the results of direct numerical simulation in comparison with analytical estimations (Bolshov, 2001 and 2006) for heat flux density distribution on a boundary are shown. As it is possible to see from figure, the good enough coincidence of numerical predictions to analytical estimations is observed.

4. VALIDATION ASPECTS

The developed technique was validated (Chudanov, 2005 and 2007) at the known numerical tests (such as heat transfer through the boundary layer, Benard convection, 2D convection in a lid-driven cavity flow; full turbulent flow of water in a round pipe; backwards facing step flow in 2D channel) in a wide range of Rayleigh numbers from a range 10^6-10^{16} and Reynolds numbers from a range 10^2-10^4. In present paper numerical predictions were compared with experimental results of such processes as: 3D convection in a lid-driven cavity flow, 3D backwards facing step flow and T-junction thermal mixing flow. QDNS calculations were carried out on enough fine grid, i.e. the characteristic grid size was defined by Kolmogorov's scale $h \sim Re^{-3/4}$. For example, Wilcox (1993) is offered for this purpose to use the following formula $N_{DNS} \sim 0.088 Re^{9/4}$.

4.1 3D convection in a lid-driven cavity flow

In this section a cavity flow at Reynolds number of 10000 or 3D convection in a lid-driven cavity flow is considered. The width of the cavity equals a half of the length and the height of the cavity. This flow has been studied experimentally by Prasad and Koseff (1989). Figure 4 represents the results along the vertical centreline; i.e. U velocity component along Z axis and V-velocity component along Y axis are shown. Markers are experimental data; a continuous line

is numerical predictions. Numerical predictions were obtained on a grid with size 257x129x513 nodes. The good agreement of numerical prediction with experiment (Prasad, 1989) is observed (see figure 4).

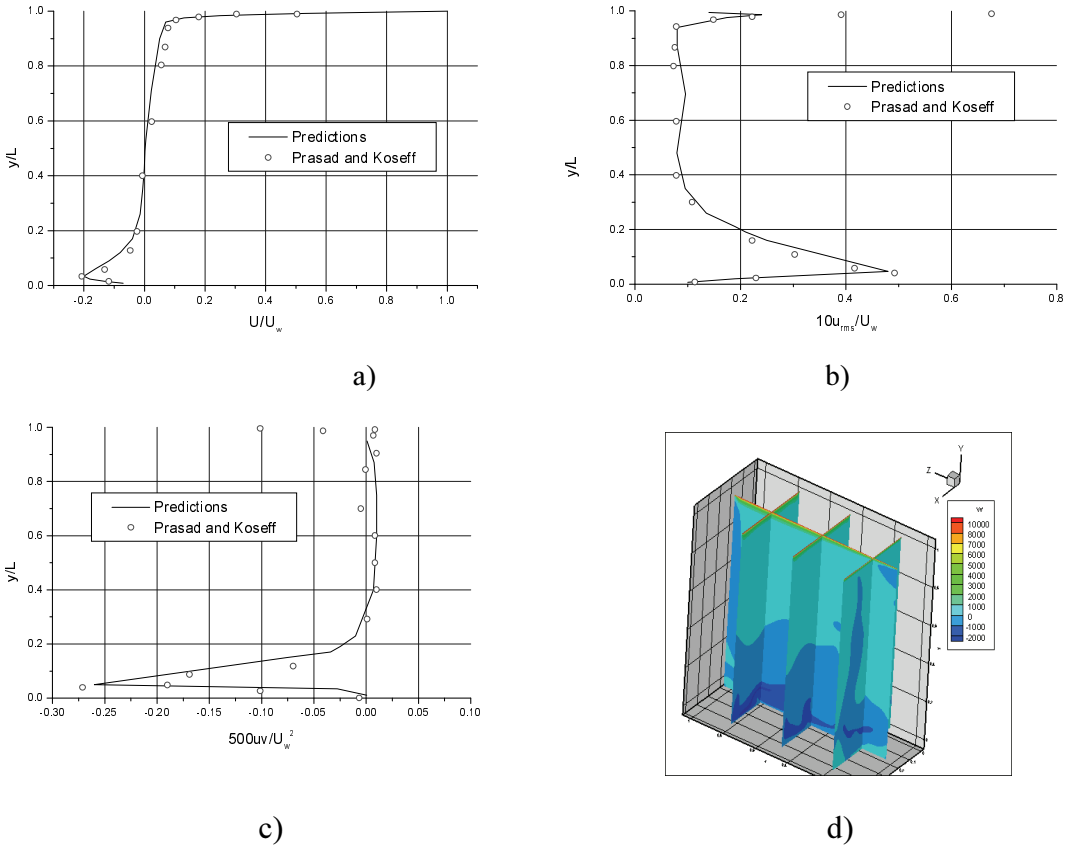

Fig. 4: Cavity flow at Re=10000. a) U/U_w -velocity (top), b) $10u_{rms}/U_w$ (middle), c) $500uv/U_w^2$ along the vertical centerline (bottom). d) 3D field of W component velocity is shown.

4.2 Full turbulent flow of water in a round pipe

The second test case is full turbulent flow of water in a round pipe over the Reynolds number from of a range 4900-25000 (Toonder, 1997). The numerical predictions and experimental results (Toonder, 1997) for Re=4900 were compared and a good agreement was obtained. Results are presented in (Chudanov, 2005).

4.3 Backwards facing step flow at $\mathrm{Re}_h = 5100$

The BFS simulations concerned the flow over a BFS of height h, with a turbulent oncoming boundary layer of thickness $\delta = 1.2h$ and free stream velocity u_∞. For all cases an inlet section of $L_i = 10$ (dimensionless length) was added before the step. The total size of the computational domain for all cases was $(L_i + L_x, L_y, L_z) = (30,4,6)$ with the step covering the 1/6 of the total size of the domain in z direction. Thus the free surface was located at a distance 6h in accordance with the experimental data of Jovic and Driver (1994). The reattachment length X_r was the basic parameter of comparison with the reference data. For the experimental data (Jovic, 1994) X_r=6.0h-6.1h. Due to the instantaneous character of the simulation the reattachment point can be located only in a time-averaged fashion. Figure 5a and 5b shows the comparison with experimental data of the mean field for the streamwise (U) and normal velocity (W) components. At figure 5c the three-dimensional field of W velocity component for BFS flow is presented.

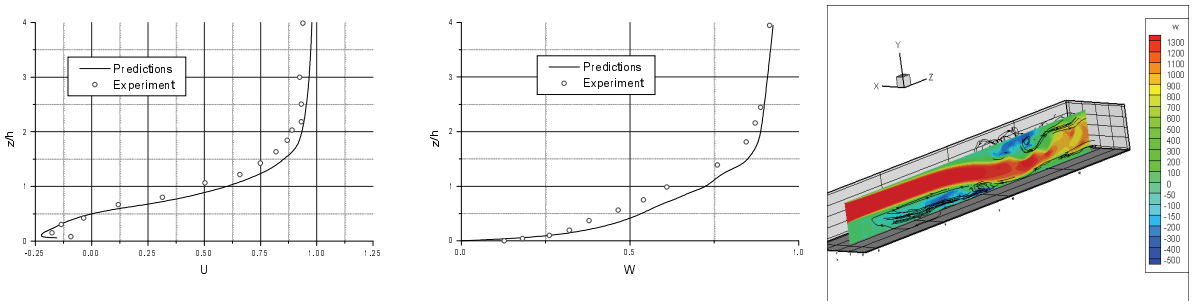

a) b) c)

Fig. 5: a) a mean field for the streamwise; b) normal velocity (W); c) 3D field of W velocity component for BFS flow.

4.4 T-junction thermal mixing flow

In this section the results of numerical simulation of thermalhydraulics at T-junction thermal mixing are submitted. A test's singularity is that the hot flux from a vertical pipe is poured into a horizontal pipe with a cold flux. At figure 6a the calculated geometry for modeling T-junction thermal mixing flow is shown. At figure 6b the fluctuations of the u-velocity component with comparison to Westion (2008) is presented. As can see from figure, a good agreement is observed.

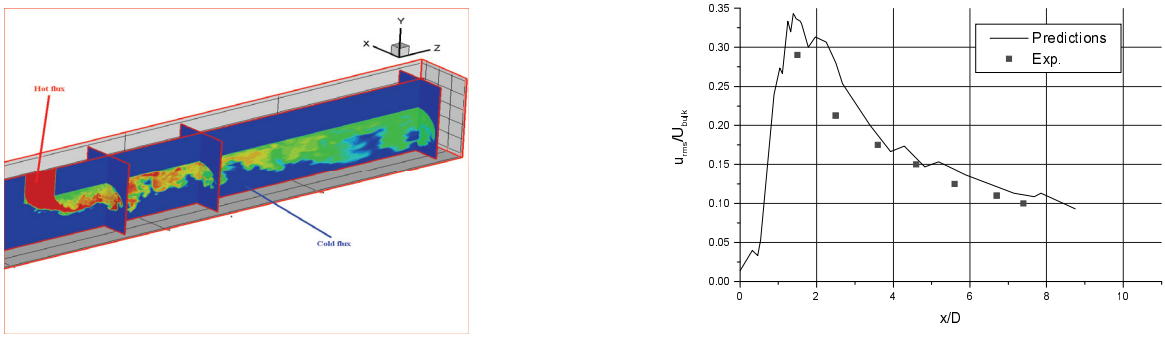

a) b)

Fig. 6: a) Calculation domain; b) fluctuations of the u-velocity component.

Moreover, the IBRAE numerical predictions and results (Mahaffy, 2010) were compared (see figs 7-10). In first case IBRAE predictions are obtained at grid with 12 million nodes and marked by a dashed line (12M). In second case IBRAE predictions are obtained at grid with 40 million nodes and marked by a solid line (40M). Mahaffy predictions (2010) were obtained at grid with 7 million nodes and marked by stars (7M). Experimental data are marked by circles.

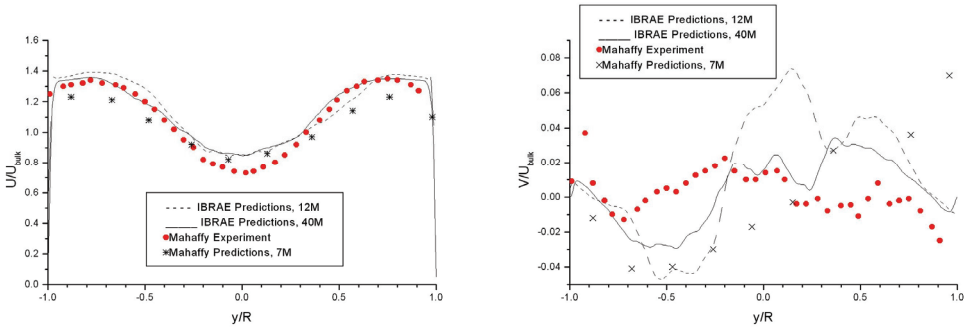

a) b)

Figure 7: Time averaged values for U - (a) and V - (b) versus y/R at x/D=1.6.

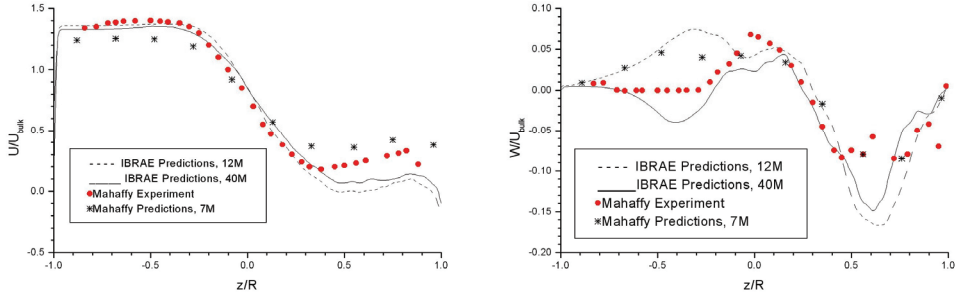

a) b)

Figure 8: time averaged values for U - (a) and W – (b) versus z/R at x/D=1.6.

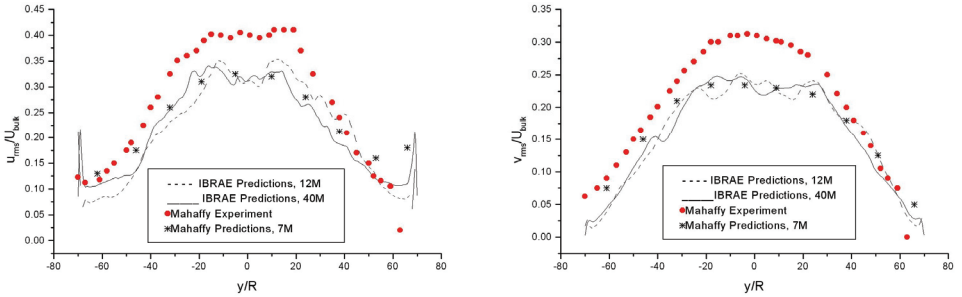

a) b)

Figure 9: RMS of the velocity x - (a) and y - (b) component fluctuations versus z/R at x/D=1.6.

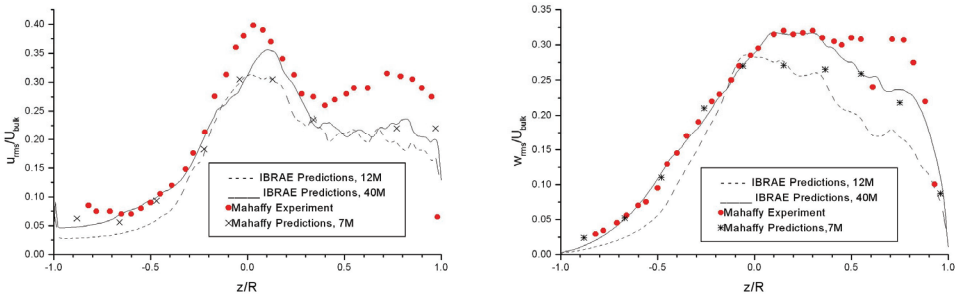

a) b)

Figure 10: RMS of the velocity x and z component fluctuations versus z/R at x/D=1.6.

A coincidence of numerical predictions and experiment is satisfactory. Failure to take account of some effects and usage of a rough grid are responsible for the observed divergence.

5. MODELING OF THE FUEL ASSEMBLIES

The successful validation of developed methodology allows its usage for industrial applications, namely for modeling of the fuel assemblies. The demonstrated example was carried out for research of a hydraulic resistance factor of a grid spacer. For numerical simulation the data (http://www.atominfo.ru/news/air1749.htm) were used (see figure 11).

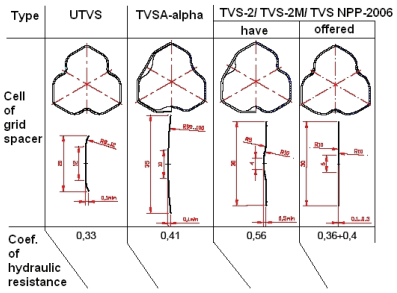

Fig. 11: Grid spacers (http://www.atominfo.ru/news/air1749.htm).

At figures 12 the geometry obtained by means of 3dsMax version 7 is shown. Below in tables 2-3 the coefficient of hydraulic resistance of grid spacer and pressure gradient at kinematic viscosity $\nu=10^{-6}$ m^2/s are presented, which were calculated for fuel assembly from 19 rods and 5 grid spacers (fig.12). The hydraulic diameter for calculations without grid spacer is equal to 10 millimeters. The hydraulic diameter for calculations with grid spacer is equal to 3 millimeters.

Table 2: Hydraulic resistance coefficient of a grid spacer

Velocity, m/s	*Without rods*		*With rods*
3	0.33 (exp.)	0.32	0.8
6	-	0.31	0.73
10	-	0.30	0.66

Table 3: Pressure gradient

Velocity, m/s	*Without grid spacer, kPa per meter*
3	8
6	30
10	60

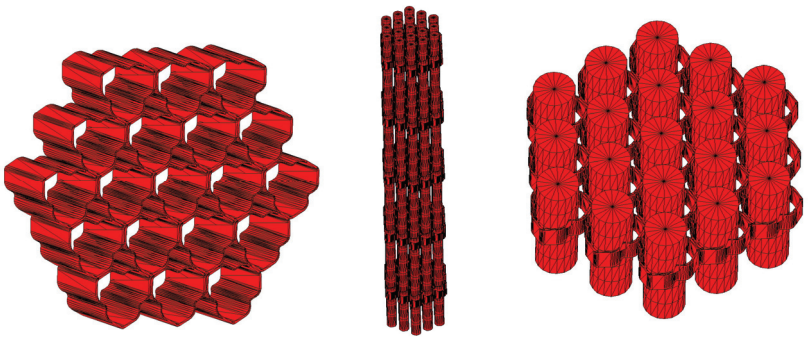

a) b) c)

Fig. 12: A grid spacer: a) isometric view; b) fuel assembly from 19 rods and 5 grid spacers, c) fragment of fuel assembly wit grid spacer.

The geometry similar to UTVS was used in calculations. The results were carried out on a sequence of grids 10^7-10^8 nodes and the convergence on a sequence of grids was obtained.

In figures 13 and 14 the diagrams of vorticity and pressure along the Z-axis are shown depending on a grid step. As it is visible from figures, with a refinement of the grid step the convergence is increased.

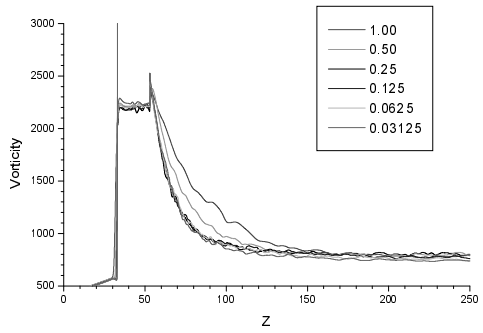

Fig. 13: diagrams of a vorticity along Z-axis versus a grid step.

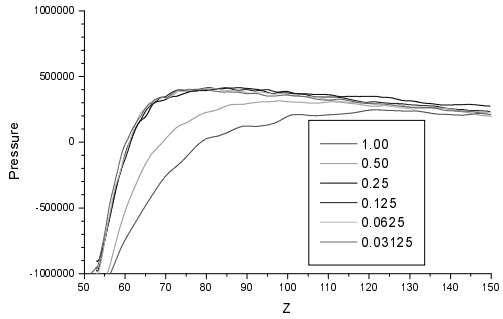

Fig. 14: diagrams of a pressure along Z-axis versus a grid step.

CONCLUSIONS

For 3D simulation of various thermalhydraulic processes on NPP in a wide range of parameters ($Ra < 10^{16}$ and $Re=10^{3}$-10^{4}) the 3D unified numerical thermalhydraulic technique and 3D CFD code for safety analysis of the operated NPPs were developed.

The developed technique was tested in area of turbulent flows, for which the good qualitative and quantitative coincidence with numerical QDNS predictions was obtained. All numerical predictions were obtained without any turbulence model. The numerical simulation results of both test problems and calculations about a fuel assembly fragment with a grid spacer allow speaking about a possibility of QDNS of thermalhydraulic in fuel assembly with the help of the developed numerical approach.

REFERENCES

1. L.A. Bolshov, P.S. Kondratenko, V.F. Strizhov, “A semi-quantitative theory of convective heat transfer in a heat generating fluid”, *Int. J. Heat and Mass Transfer*, Vol. 41, №10, 1223-1227 (1998).
2. L.A. Bolshov, P.S. Kondratenko, V.F. Strizhov,”Buoyancy-induced convection of heat generating liquid”, *J. Uspehi Fiz. Nauk*, Vol. 171, №10, 1051-1070 (2001).
3. L.A. Bolshov, V.V. Chudanov, et al., “Best estimate methodology for modeling bubble flows”, *Proc. ICONE14. 14th International Conference on Nuclear Engineering,* Miami, Florida, USA. July 17-20, 2006*,* CD-disk, paper №ICONE-89296 (2006).
4. V.V. Chudanov, et al., “Current status and validation of CONV2D\&3D code”, *Proc. OECD/CSNI Workshop on in vessel core debris retention and coolability,* Garching near Munich, Germany, March 3-6. 1998. Nuclear Safety NEA/CSNI/R(98) 18, pp. 223-234 (1999).

5. V.V. Chudanov, et al., “A multi-block orthogonal grid generation using CAD system”, *Proc. 8th International Meshing Roundtable,* South Lake Tahoe, California, October 10-13. 199. USA, Sandia Report, SAND 99-2288, pp. 179-186 (1999).
6. V.V. Chudanov, et al. *J. of computing mathematics and of mathematical physics*, Vol.40, № 6, 900-907 (2001).
7. V.V. Chudanov, A.E. Aksenova, V.A. Pervichko, “3D unified CFD approach to thermalhydraulic problems in safety analysis”, *Proc. of IAEA Technical Meeting on Use of Computational Fluid Dynamics (CFD) Codes for Safety Analysis of Nuclear Reactor Systems, Including Containment,* University of Pisa, Italy, 11-14 November, 2002. (CD-disk (Session 7). Summary reports IAEA-TECDOC-1379. p.14 (2003).
8. V.V. Chudanov, A.E. Aksenova, V.A. Pervichko, “CFD to modelling molten core behaviour simultaneously with chemical phenomena”, *Proc. 11th International Topical Meeting on Nuclear Reactor Thermal-Hydraulics (NURETH-11),* Popes’ Palace Conference Center, Avignon, France, October 2-6, 2005. CDROM, paper №048 (2005).
9. V.V. Chudanov, A.E. Aksenova, V.A. Pervichko, “Methods of direct numerical simulation of turbulence in thermalhydraulic’s problems of fuel assembly”. *Izvestiya Rossiiskoi Akademii Nauk. Seriya Energetica*, №6, 47-57 (2007).
10. S. Jovic, D.V. Driver, “Backward-facing step measurement at low Reynolds number”, *NASA Technical memorandum*, No.108807 (1994).
11. S. Modro, M. El-Shanawany, and S. Lee, “Recent IAEA activities in support of safety assessment capabilities”, *Proc. of ICONE14 International Conference on Nuclear Engineering*, Miami, Florida, USA. July, 17-20, 2006, CD-disk, paper №ICONE-89828 (2006).
12. A. Prasad and J. Koseff, “Reynolds Number and End-Wall Effects on a Lid- Driven Cavity Flow”, *J. Physics of Fluids A*, Vol. 1, № 2, 208–218 (1989).
13. J.M.J. den Toonder and F.T.M Nieuwstadt, “Reynolds Number Effect in a Turbulent Pipe Flow for Low to Moderate Re”, *J. Phys. Fluids*, Vol.9, №11, 3398-3409 (1997).
14. J. Westin, P. Veber, L. Andersson, C. Mannetje, U. Andersson, J. Eriksson, M. Henriksson, F.Alavyoon, C. Andersson, “High-cycle thermal fatigue in mixing Tees. Large-eddy simulations compared to a new validation experiment”. *Proc. 16th International Conference on Nuclear Engineering*. Orlando, USA, May 11–15, 2008. ICONE16-48731 (2008).
15. D.C. Wilcox, *Turbulence modelling for CFD*, DCW Industries, USA, Glendale California. ISBN 0-9636051-0-0 (1993).
16. http://www.atominfo.ru/news/air1749.htm.
17. John Mahaffy and Brian Smith, Synthesis of Benchmark Results, OECD/NEA T-JUNCTION BENCHMARK, 2010.